JOURNAL OF COMPUTATIONAL PHYSICS 109, 93–107 (1993)

The Hyperelliptic Inverse Scattering Transform for the Periodic, Defocusing Nonlinear Schroedinger Equation

A. R. OSBORNE

Istituto di Fisica Generale dell'Università, Via Pietro Giuria 1, Torino 10125, Italy

Received June 26, 1992; revised March 11, 1993

The nonlinear Schroedinger (NLS) equation describes the spatio-temporal evolution of the complex envelope function of a narrow-banded, nonlinear wave train. Here I exploit the nonlinear Fourier structure of NLS, known as the inverse scattering transform, to study nonlinear periodic modulations in the spectral domain. Numerical algorithms are presented for both the direct and inverse scattering transforms of the "defocusing" NLS equation with *periodic boundary conditions*. A discrete algorithm is given for computing the monodromy matrix of periodic spectral theory and the *direct scattering transform* is then computed from the elements of this matrix. A fast algorithm for the *inverse scattering transform* in terms of the hyperelliptic function representation is also given; solutions to the defocusing NLS equation are determined by a linear superposition of these nonlinear oscillation modes. The direct algorithm uses computer time proportional to M^2, where M is the number of points in the discrete envelope function of the wave train. The inverse scattering algorithm is "fast" in the sense that it is M^3; this contrasts to the periodic theta-function inverse problem for NLS which is M^4 and to the Gelfan'd–Levitan–Marchenko integral equation for infinite-line boundary conditions which is also M^4. Several wave train solutions of NLS are considered and their inverse scattering transform spectra and nonlinear Fourier decompositions are discussed. Application of the method to the analysis of computer generated or experimentally measured space or time series is the major motivation for this work.

I. INTRODUCTION

The classic paper by Ablowitz, Kaup, Newell, and Segur (AKNS) [1] synthesized a fundamental new idea in the field of theoretical soliton physics. Their approach, which they called the *inverse scattering transform* (IST), evolved from the pioneering work of Gardner, Greene, Kruskal, and Muira (GGKM) [2] and Zakharov and Shabat [3]. The essential idea is that IST is a *nonlinear generalization of the ordinary linear Fourier transform* to the solution of particular *nonlinear* partial differential (wave) equations (PDEs) with infinite-line boundary conditions. Nonlinear integrable PDEs of this type include the Korteweg–deVries (KdV), the nonlinear Schroedinger (NLS), sine-Gordon, sinh-Gordon, and modified Korteweg–deVries equations. GGKM solved the KdV equation using a linear integral equation due to Gelfan'd, Levitan, and Marchenko (GLM) [4]; a key step in their approach was to associate a particular (spectral) eigenvalue problem, the time-independent Schroedinger equation of quantum mechanics, with KdV. Zakharov and Shabat applied a similar technique to the nonlinear Schroedinger equation [3], for a different eigenvalue problem, and found the exact spectral solution to NLS in terms of two coupled GLM-type equations. AKNS then generalized the method to a large class of wave equations in one space and one time $(1+1)$ dimensions for infinite-line boundary conditions. The theoretical formulation of IST has since been extended to include *periodic boundary conditions* for a considerable number of nonlinear PDEs, including the KdV, NLS, sine-Gordon, and sinh-Gordon equations [5–12]. For recent reviews on inverse scattering theory and its application to the solution of integrable PDEs the reader is referred to the literature [4, 13–16].

The triumph of the soliton theories is undisputed; a large number of fully nonlinear wave equations are known to be integrable (fully solvable) in terms of the inverse scattering transform. The focus in the present paper is to use IST (1) to better understand the spectral and physical structure of the nonlinear Schroedinger equation and (2) to develop numerical algorithms for the nonlinear Fourier analysis of computer generated or experimental data. Much of the motivation of this work comes from recent successes in the development of algorithms for the KdV equation [17–30] and for the subsequent analysis of surface wave data from both the laboratory and the ocean [17, 29–31]. In this context *periodic boundary conditions* are of primary interest because stationarity and ergodicity must often be ensured in an experimental context. Furthermore, since computer generated signals are necessarily discrete, compatibility with the finite-term, discrete Fourier transform is required [25, 27]. These conditions are met for the algorithms developed herein.

Given that periodic boundary conditions are important

0021-9991/93 $5.00

in many physical applications, a number of investigators have developed numerical methods for obtaining the periodic scattering transform of space or time series [20, 23–28, 32–41]. An important consideration is the fact that nonlinear integrable systems with periodic boundary conditions have *nonlinear basis functions* (the *nonlinear oscillation modes* of the PDE) which describe the dynamics of complex wave trains. Periodic IST provides the solution to the wave equations in terms of a *linear superposition* of the nonlinear modes, referred to as the hyperelliptic-function representation [5–12, 15]; linearization of the hyperelliptic functions by the Jacobian transformation of algebraic geometry leads to the "theta function" inverse problem [5–12], an alternative approach to solving an integrable, nonlinear PDE which is a periodic analogue of the infinite-line GLM equation. It is worth noting that the nonlinear periodic theories are formulated in such a way as to easily reduce to ordinary linear *Fourier series* for small amplitude wave motion [18, 19]. Thus the nonlinear theoretical formulation given herein automatically includes the mathematics of linear Fourier series.

The nonlinear Schroedinger equation was solved for periodic boundary conditions by Ma and Ablowitz [11]. NLS describes the nonlinear space/time evolution of the *envelope* of a narrow-banded wave train, in which two cases are of physical relevance: (1) the *defocusing case*, which is essentially a multi-scale reduction of the KdV equation to narrow-banded wave trains [21, 22, 24, 42] and (2) the *focusing case*, where *envelope solitons* can form and propagate [43–48]. In the present work interest rests primarily with the defocusing case; the focusing case will be covered in a later paper. The periodic IST for defocusing NLS parallels that of the KdV equation in many respects, with some variations which are discussed below.

The major results of the present paper are the development of *numerical algorithms for both the direct and inverse scattering problems for periodic boundary conditions*. While a number of investigators have developed algorithms for the direct scattering problem [32–41], the approach given herein provides for the first time a general numerical tool for reconstructing the potential by the inverse scattering problem. The present inverse algorithm has particular speed advantages over the periodic theta function inverse problem [11] and the Gelfan'd–Levitan–Marchenko integral equation in the formulation of NLS with infinite-line boundary conditions. From a practical point of view the periodic algorithm presented here for the inverse scattering problem uses computer time proportional to M^3 (M is the number of discrete points in the modulation envelope), while the standard approach to the numerical solution of the GLM equation is M^4; likewise the periodic theta function inverse problem (an alternative to the hyperelliptic function representation used here) is M^4. For a typical time series of $M = 1000$ points this implies an improvement of roughly 1000 in computational speed using the approach given herein. A further advantage is that one can *explicitly compute each of the nonlinear oscillation modes of periodic theory*, whereas the theta function inverse problem and the infinite-line GLM equation cannot easily be exploited for this purpose. Here I present mutually complimentary algorithms for (a) the computation of the nonlinear oscillation modes of an input wave train and (b) the subsequent reconstruction of the wave train by a linear superposition law. These theoretical and numerical tools have been recently applied to a related PDE, the KdV equation, to analyze and nonlinearly filter measured time series of complex wave motions from both the laboratory and the ocean [29–31].

The methods given here may be thought of as *time series analysis techniques*. They are fully discrete, exact approaches to the scattering transform spectral problem and to the associated hyperelliptic-funcion inverse problem for a *piecewise constant wave train* (Fig. 1). The perspective given here contrasts (a) to other methods which might be thought of as being purely numerical [33, 35, 36] (i.e., those based upon numerical integration of the spectral eigenvalue problem by, say, a higher-order Runge–Kutta algorithm) or (b) to alternative approaches which are purely discrete solutions to the scattering problem associated with a *discrete*

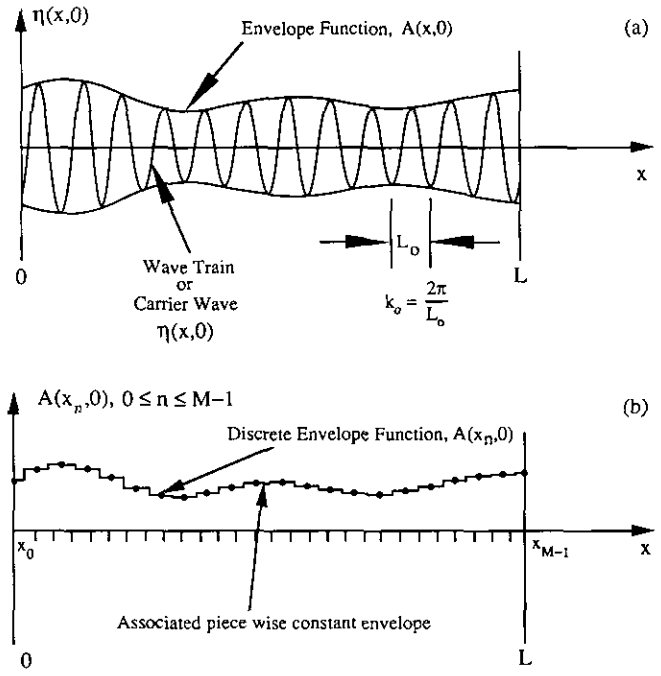

FIG. 1. (a) A narrow-banded periodic nonlinear wave train $\eta(x, 0)$ with complex envelope $q(x, 0) = A(x, 0) \exp[i\phi(x, 0)]$ is assumed to be given as a function of x at time $t = 0$. Note that the wave train is localized on the spatial interval $(0, L)$. The wave train of (a) is discretized at intervals Δx and, with the aid (say) of the Hilbert transform, a discrete envelope function $A(x_n, 0)$ $(0 \le n \le M-1)$ is computed (b) (dots). In order to determine the scattering transform the discrete envelope is replaced by a piece wise constant function (b). The direct scattering transform algorithm given herein is analytically exact for wave envelopes of this latter type.

NLS equation ([53], see also [32, 32, 34, 37–41] and Section 5 below). The fact that the numerical approach given here simultaneously (a) is purely discrete, (b) provides a relatively fast inverse problem (M^3), and (c) has certain numerical advantages over integrable methods [11] means that space and time series, with their requisite thousands of degrees of freedom, can be analyzed with considerable ease. These new methods have been shown to be useful in the analysis of laboratory and oceanic wave data, where long time series of 1000 to 10000 points are common and where experimental noise must be accounted for [25–27, 29–31].

It is worthwhile giving some perspective about the methods given herein with regard to the analysis of data using the well-known linear Fourier transform. For the analysis of space or time series one has essentially two numerical tools, one the *direct*, the other the *inverse* Fourier transform. The direct algorithm allows one to determine the Fourier spectrum as an aid to the interpretation of data. The inverse algorithm allows one (a) to reconstruct the input time series from the Fourier spectrum or (b) to filter the data, i.e., to remove certain (often high) frequencies and to reconstruct the time series in the absence of these frequencies. The latter application is particularly important in the removal of high frequency noise which may be present in the data. The spirit of the present paper is to develop analogous tools for the *nonlinear* Fourier analysis of data, here assumed to behave approximately like the NLS equation. This paper gives algorithms for both the direct and inverse scattering transforms for NLS. One is thus able to compute the spectrum from the direct transform and to reconstruct the input space or time series from the inverse transform. In the latter operation one may also *nonlinearly* filter the data, i.e., selectively remove particular frequency components in the spectral domain, in the presence of nonlinear interactions, and reconstruct the time series in the absence of these components. Nonlinear filtering as a useful tool for eliminating certain kinds of experimental noise is discussed elsewhere [25–27, 29–31].

The rest of this paper is organized as follows: in Section II I briefly discuss the periodic NLS equation and its physical behavior. Section III is devoted to a discussion of IST for periodic NLS in the defocusing regime. In Section IV numerical algorithms are given for both the direct and inverse scattering transforms. In Section V the numerical results and their associated physical implications are presented.

II. THE NONLINEAR SCHROEDINGER EQUATION FOR PERIODIC BOUNDARY CONDITIONS

Generally speaking the nonlinear Schroedinger equation can be written in the dimensionless form

$$iq_t - q_{xx} + 2\sigma |q|^2 q = 0, \tag{2.1}$$

where $q(x, t)$ is the complex envelope function of a carrier wave of wavenumber k_0 (Fig. 1). The physically significant coefficient $\sigma = (\pm 1)$ lies before the nonlinear cubic term in the equation. Depending upon the sign σ there are two regimes of the motion. The so-called *focusing regime* ($\sigma = -1$) admits non-dispersive stable solutions such as solitons and "breather" trains. In the *defocusing regime* ($\sigma = +1$) soliton solutions do not occur; the motion is nevertheless still quite rich in terms of nonlinear effects; this is the case considered herein.

The nonlinear Schroedinger equation is a generic, integrable wave equation in the sense that it arises in many physical contexts as the first modulation correction to a wave train in a nonlinear medium in $1 + 1$ dimensions. For example, NLS has been derived in the context of water waves, plasma physics, nonlinear optics, etc. [4].

It is well known that defocusing NLS is derivable from the KdV equation for the case $\sigma = +1$. The opposite sign $\sigma = -1$ corresponds to deep water wave motion and requires a separate derivation in its own right [44]. The value of σ is related to the water depth: the defocusing regime corresponds to shallow water ($\sigma = +1$), where one-dimensional wave trains are stable with respect to modulations of the envelope; in this sense defocusing NLS occurs in the same regime as that of the KdV equation. The relationship between the periodic spectral (scattering) theories for defocusing NLS and KdV has been extensively investigated [21, 24].

I now briefly discuss the defocusing NLS equation as it is derived from the KdV equation, which is written in dimensional form,

$$\eta_t + c_0\eta_x + \alpha\eta\eta_x + \beta\eta_{xxx} = 0. \tag{2.2}$$

Among many other applications the KdV equation describes the propagation of small, finite-amplitude, long waves in shallow water. Here $\eta(x, t)$ is the amplitude of the free surface, $c_0 = (gh)^{1/2}$ is the linear phase speed, g is the acceleration of gravity, h is the water depth, $\alpha = 3c_0/2h$ is the coefficient of the nonlinear term, and $\beta = c_0h^2/6$ is the coefficient of the dispersive term. KdV describes broad-banded wave motion; i.e., the scattering transform spectrum can cover a broad frequency range while still lying within the range of physical applicability of the equation.

The defocusing NLS equation can be derived directly from KdV (2.2) [21, 24, 42]. One assumes the Fourier spectrum is *small, but finite in amplitude* and *narrow-banded*. The nonlinear Fourier spectrum of NLS is then easy to interpret in terms of the physical behavior of the system [27]. I briefly discuss some of the major results of the derivation in order to establish the connection between the solutions to the NLS equation and the physical phenomenon in question. An asymptotic, multi-scale expansion for the

solution of the KdV equation gives a free surface elevation which has the form of a modulated Stokes wave (Fig. 1):

$$\eta(x,t) = -\frac{3A^2(x,t)}{4k_0^2h^3} + A(x,t)\cos\theta(x,t) + \frac{3A^2(x,t)}{4k_0^2h^3}\cos 2\theta(x,t) + \cdots. \quad (2.3)$$

The phase $\theta = \theta(x,t)$ is given by

$$\theta = k_0 x - (\omega_0 + \omega')t + \phi(x,t), \quad (2.4)$$

where k_0 and ω_0 are the wave number and frequency of the "carrier wave" and the associated linear dispersion relation is given by

$$\omega_0 = c_0 k_0 - \beta k_0^3.$$

The amplitude dependent, nonlinear Stokes frequency correction is

$$\omega' = \frac{9c_0\overline{A^2}}{16k_0h^4}, \quad (2.5)$$

where the overbar implies a spatial average over a single period L of the wave train. In (2.3) $A(x,t)$ is a slowly varying, real envelope function and $\phi(x,t)$ is a slowly varying real phase. In the absence of modulations $A(x,t) = A_0 = \text{const}$ and $\phi(x,t) = \phi_0 = \text{const}$ and (2.3) reduces to the familiar Stokes wave solution to KdV [49]. Generally speaking $A(x,t)$ and $\phi(x,t)$ are real functions which may be used to form a complex envelope function

$$\psi(x,t) = A(x,t)\, e^{-i\omega' t + i\phi(x,t)} \quad (2.6)$$

such that $\psi(x,t)$ is a solution to the shallow water (defocusing) dimensional *nonlinear Schroedinger* (NLS) *equation*

$$i\frac{\partial\psi}{\partial t} + iC_g\frac{\partial\psi}{\partial x} - 3\beta k_0\frac{\partial^2\psi}{\partial x^2} + \left(\frac{\alpha^2}{24\beta k_0}\right)|\psi|^2\psi = 0, \quad (2.7)$$

where $C_g = c_0 - 3\beta k_0^2$ is the group speed. In the small amplitude, narrow-banded approximation considered in this paper the theoretical formulation given by the free surface amplitude (2.3), together with the associated envelope and phase governed by NLS (2.6), (2.7) constitutes a complete, integrable theory for shallow water, nonlinear wave motion which is equivalent to the KdV equation (2.2) when the wave motion is sufficiently small in amplitude and narrow-banded. Formally speaking the solutions to these small-amplitude, narrow-banded systems do not contain solitons.

In previous work [50] we have presented a numerical algorithm for computing the nonlinear spectrum for the NLS equation with *infinite-line* boundary conditions, $q(x) \equiv q(x,0) \to 0$ as $|x| \to \infty$. Here I extend the algorithm to the case of *periodic* boundary conditions, $q(x) = q(x+L)$. This extension is useful, for example, in the analysis of water wave trains, where recorded wave data often do not asymptotically decay in space [29–31]. With periodic boundary conditions there is no time-asymptotic state as $t \to \infty$ as one has for infinite-line boundary conditions; thus the spectral components do not separate from each other asymptotically in time as they do on the infinite line [27]. This implies that the dynamics of the periodic problem in configuration space are much more complicated than the motion for infinite-line boundary conditions and the inverse scattering transform therefore becomes a valuable tool for the analysis of experimental data [29–31].

III. THE PERIODIC INVERSE SCATTERING TRANSFORM FOR THE DEFOCUSING NLS EQUATION

In the framework of the inverse scattering transform, the spectrum is obtained by solving an eigenvalue problem in which the complex envelope function $q(x,t)$ governed by NLS (2.1) acts as a "potential" in the sense of inverse scattering theory [11]. IST decomposes the original field $q(x,t)$ into a summation of nonlinear basis functions (hyperelliptic oscillation modes) that are strongly interacting functions of space and time. In the linear (small amplitude, $q \to 0$) limit these modes reduce to the independent linear sinusoidal components of an ordinary Fourier series [19, 20]. In this sense one can think of periodic IST as a generalization of Fourier series.

I now briefly discuss periodic scattering theory for NLS [11]. The spectral eigenvalue problem is

$$\Psi_x(x,\zeta) = \mathbf{A}\Psi(x,\zeta), \quad (3.1)$$

where $\Psi(x,\zeta) = \begin{pmatrix}\psi_1(x,\zeta)\\ \psi_2(x,\zeta)\end{pmatrix}$ is a two-component complex eigenfunction and $\mathbf{A}$ is the matrix

$$\mathbf{A} = \begin{pmatrix} -i\zeta & q \\ q^* & i\zeta \end{pmatrix}; \quad (3.2)$$

ζ is the complex spectral wavenumber, $q \equiv q(x,0)$ is the complex solution of NLS (2.1) at time $t = 0$, and the $*$ denotes complex conjugate. Here, and in the sequel, one drops the time dependence from $q(x,t)$ because of the parametric character of time in the direct spectral problem (3.1), (3.2). This is consistent with the fact that IST solves the Cauchy problem for NLS (2.1); e.g., the spectrum of $q(x,0)$ is determined from (3.1), (3.2) and is then evolved forward in time by the inverse problem (see [11] and below).

I now briefly discuss the periodic spectrum associated with the above spectral problem and refer the interested reader to the literature for further details [11]. For Ψ a solution of (3.1), another solution is given by

$$\Psi' = \begin{pmatrix} \psi_2^*(x, \zeta^*) \\ \psi_1^*(x, \zeta^*) \end{pmatrix}. \tag{3.3}$$

One fixes a basis by normalizing the two eigenfunctions Ψ, Ψ' of (3.1) at some arbitrary base point x_0 in such a way as to ensure independence. To this end the following simple normalization is used:

$$\begin{aligned} \Psi(x_0, \zeta) &= \begin{pmatrix} 1 \\ 0 \end{pmatrix} \\ \Psi'(x_0, \zeta) &= \begin{pmatrix} 0 \\ 1 \end{pmatrix}. \end{aligned} \tag{3.4}$$

Due to the periodicity of the potential $q(x)$, $\Psi(x+L, \zeta)$ will also be a solution of (3.1) which can be expanded in terms of the basis (3.4),

$$\Psi(x+L, \zeta) = a(\zeta)\, \Psi(x, \zeta) + b(\zeta)\, \Psi'(\zeta, x), \tag{3.5}$$

where $a(\zeta)$ and $b(\zeta)$ are called the *scattering coefficients* and define (together with their complex conjugates) the so-called *monodromy matrix*,

$$\mathbf{S}(\zeta, x_0) = \begin{pmatrix} a(\zeta) & b^*(\zeta^*) \\ b(\zeta) & a^*(\zeta^*) \end{pmatrix} \tag{3.6}$$

Evaluating (3.5) at $x = x_0$ and using (3.4) gives

$$\begin{aligned} a(\zeta, x_0) &= \psi_1(x_0 + L, \zeta) \\ b(\zeta, x_0) &= \psi_2(x_0 + L, \zeta). \end{aligned} \tag{3.7}$$

Using the normalization (3.4) further implies:

$$\det \mathbf{S}(\zeta) = a(\zeta)\, a^*(\zeta^*) - b(\zeta)\, b^*(\zeta^*) = 1. \tag{3.8}$$

A useful decomposition of an arbitrary function $f(\zeta)$ is given by

$$\begin{aligned} f_R(\zeta) &= \frac{1}{2}\,(f(\zeta) + f^*(\zeta^*)) \\ f_I(\zeta) &= \frac{1}{2i}\,(f(\zeta) - f^*(\zeta^*)) \end{aligned} \tag{3.9}$$

and is employed below. Equations (3.9) reduce to the ordinary real and imaginary parts of $f(\zeta)$ whenever $\zeta \in \mathbf{R}$.

The three kinds of IST spectrum are given by the following conditions:

The *main spectrum* $\{\zeta_j\}$ is given by the simple roots of

$$a_R^2(\zeta_j) = 1, \qquad 1 \leqslant j \leqslant 2N. \tag{3.10}$$

The *first auxiliary spectrum* $\{\gamma_i\}$ is defined by

$$a_I(\gamma_i) + b_I(\gamma_i) = 0, \qquad 1 \leqslant i \leqslant N. \tag{3.11}$$

The *second auxiliary spectrum* $\{\eta_i\}$ is defined by

$$a_I(\eta_i) + b_R(\eta_i) = 0, \qquad 1 \leqslant i \leqslant N. \tag{3.12}$$

The space/time invariant main spectrum $\{\zeta_j\}$, $1 \leqslant j \leqslant 2N$, is a solution to (3.10). The auxiliarly spectrum $\{\gamma_i\}$, $\{\eta_i\}$, $1 \leqslant i \leqslant N$, corresponds to those values of ζ which satisfy (3.11) and (3.12). Here N is the number of "open bands" or "degrees of freedom" in the theory. The general solutions to NLS are then constructed as nonlinear Fourier series with exactly N terms ((3.16) below); these are then "N-band potentials" in the terminology of periodic scattering theory [5–12].

Several properties associated with the scattering spectra (3.10)–(3.12) [11] are now given. The spectra $\{\zeta_j\}$, $\{\gamma_i\}$, and $\{\eta_i\}$ are all real and generally depend both on the reference point x_0 and on the time parameterization (since q is a function of both x and t). The *isospectrality of the scattering problem* means that as the potential $q(x, t)$ obeys the space-time evolution of the NLS equation the following fundamental property holds:

$$\frac{\partial a_R}{\partial x_0} = \frac{\partial a_R}{\partial t} = 0. \tag{3.13}$$

This means that the main spectrum $\{\zeta_j\}$ (3.10) is constant in both space and time.

The auxiliary spectra $\{\gamma_i, \eta_i\}$ are instead dependent on space and time and are referred to as the *nonlinear oscillation modes* of the theory. The spatial dependence x_0 of $\{\gamma_i, \eta_i\}$ is governed by two sets of coupled, nonlinear ordinary differential equations:

$$\begin{aligned} \frac{\partial \gamma_i}{\partial x_0} &= \frac{2\sigma_i \sqrt{-R(\gamma_i)}}{\prod_{k \neq i}^{N} (\gamma_i - \gamma_k)} \left(\sum_{k \neq i}^{N} \gamma_k - \frac{1}{2} \sum_{j=1}^{2N} \zeta_j \right) \\ \frac{\partial \eta_i}{\partial x_0} &= \frac{2\delta_i \sqrt{-R(\eta_i)}}{\prod_{k \neq i}^{N} (\eta_i - \eta_k)} \left(\sum_{k \neq i}^{N} \eta_k - \frac{1}{2} \sum_{j=1}^{2N} \zeta_j \right), \end{aligned} \tag{3.14}$$

where σ_i, $\delta_i = \pm 1$ (they are the signs of the square roots in (3.14)) and

$$R(\zeta) = \prod_{j=1}^{2N} (\zeta - \zeta_j). \tag{3.15}$$

Equations (3.14) nonlinearly couple all the Fourier components $\{\gamma_i, \eta_i\}$ and give rise to quite complex dynamics for defocusing NLS, as will be seen in the numerical examples discussed below.

In this paper the explicit time evolution of the $\{\gamma_i, \eta_i\}$ is not considered; this evolution is governed by nonlinear ordinary differential equations given elsewhere [11]. All numerical calculations made herein may be viewed as occurring at some arbitrary fixed time t_0. One thus computes the $\{\gamma_i, \eta_i\}$ as a function of x_0 in order to reconstruct (from the spectrum) an arbitrary input wave train at the fixed time t_0.

The segment on the ζ axis between two band edges (where $a_R^2(\zeta) \geqslant 1$) defines an *open band* or *degree-of-freedom* of the motion. The auxiliary spectra $\{\gamma_i, \eta_i\}$ lie inside the open bands as they vary as a function of (x, t) and there is one and only one γ_i and η_i for each open band. It is assumed in the following that the potential $q(x)$ gives rise to a *finite number* N of open bands so that $1 \leqslant i \leqslant N$. The scattering spectrum is thus defined by $4N$ real quantities $\{\zeta_j, 1 \leqslant j \leqslant 2N; \gamma_i, \eta_i, 1 \leqslant i \leqslant N\}$. The theoretical restriction to N bands implies that there are exactly N terms in the nonlinear Fourier series expansion for the NLS equation as is now discussed.

Knowing the spectrum $\{\zeta_j, \gamma_i, \eta_i\}$ for every x and t_0 allows reconstruction of the input potential by means of a simple linear superposition law which is referred to as the *inverse scattering transform*:

$$\begin{aligned} q_R(x, t_0) &= -\tfrac{1}{2} \sum_{j=1}^{2N} \zeta_j + \sum_{i=1}^{N} \eta_i(x, t_0) \\ q_I(x, t_0) &= \tfrac{1}{2} \sum_{j=1}^{2N} \zeta_j - \sum_{i=1}^{N} \gamma_i(x, t_0). \end{aligned} \tag{3.16}$$

These formulas are essentially nonlinear Fourier series for the real and imaginary parts of the solution to NLS, $q(x, t_0)$.

What are the implications of constructing potentials from *exactly* N bands on the analysis of space and time series which have M discrete points? This problem was considered by Osborne and Bergamasco [18] for the KdV equation and by Osborne [19] for defocusing NLS. Essentially one find that a space/time series of exactly M points is described by an $N = M$ band potential. This parallels linear Fourier analysis; i.e., a discrete function of M points has exactly M terms in its associated Fourier series.

IV. THE NUMERICAL APPROACH AND ITS IMPLEMENTATION

The Algorithm

I now discuss numerical algorithms for the computation of the direct and inverse scattering transforms for NLS. These algorithms are extensions of previous work for the infinite-line and periodic KdV equations [18–28] and for the NLS equation on the infinite line [50].

I first address the direct algorithm, which uses a piecewise constant discretization of the wave envelope function $q(x)$ into M constant values q_n $(0 \leqslant n \leqslant M-1)$ at spatial values $x_n = n\,\Delta x$, with discretization intervals $\Delta x = L/M$ (Fig. 1). Here L is the period of the envelope function, $q(x+L) = q(x)$, so that $q_{M+1} = q_1$. The integration of the Schroedinger equation (3.1) in a particular interval Δx gives $\psi(x_n) = \exp(\mathbf{A} x_n)$, so that

$$\Psi(x_n + \Delta x) = \Psi(x_{n+1}) = \mathbf{U}(q_n)\, \Psi(x_n) \tag{4.1}$$

for $\Delta x = x_{n+1} - x_n$. The matrix $\mathbf{U}(q)$ is found from the matrix $\mathbf{A}$ (3.2) by

$$\begin{aligned} \mathbf{U}(q) = \exp[\Delta x\, \mathbf{A}] &= \exp\begin{pmatrix} -i\zeta & q \\ q^* & i\zeta \end{pmatrix} \Delta x \\ &= \begin{pmatrix} \cosh(\kappa\,\Delta x) - \dfrac{i\zeta}{\kappa}\sinh(\kappa\,\Delta x) & \dfrac{q}{\kappa}\sinh(\kappa\,\Delta x) \\ \dfrac{q^*}{\kappa}\sinh(\kappa\,\Delta x) & \cosh(\kappa\,\Delta x) + \dfrac{i\zeta}{\kappa}\sinh(\kappa\,\Delta x) \end{pmatrix} \end{aligned} \tag{4.2}$$

and $\kappa^2 = qq^* - \zeta^2$.

The solution of the scattering problem is constructed over one period $(0 \leqslant x \leqslant L)$ from the contributions due to matrices for each interval Δx. It follows from (4.1) that, taking the product of M matrices (4.2),

$$\Psi(x_M) = \prod_{n=M-1}^{0} \mathbf{U}(q_n)\, \Psi(x_1), \tag{4.3}$$

and using the normalization (3.4), the monodromy matrix $\mathbf{S}(x_0)$ is then defined by

$$\mathbf{S}(x_0) = \prod_{n=M-1}^{0} \mathbf{U}(q_n), \tag{4.4}$$

where x_0 is an *arbitrary* base point in the interval $(0, L)$. Thus $\mathbf{S}(x_0)$ is seen to carry the solution one period $x_M = L$ from $\Psi(x_0)$ to $\Psi(x_0 + x_M)$ to satisfy the periodic boundary conditions. According to (3.6), (3.7),

$$\begin{aligned} a(\zeta, x_0) &= S_{11} \\ b(\zeta, x_0) &= S_{21}. \end{aligned} \tag{4.5}$$

It is worth noting that the matrices $\mathbf{U}(q)$ and $\mathbf{S}(x_0)$ have determinants equal to one, so the relation (3.8) for the scattering coefficients is automatically satisfied due to the form of (4.3).

The periodic spectra are then given as the solution to the equations

Main spectrum. The $\{\zeta_j\}$, $1 \leqslant j \leqslant 2N$, are the solutions of

$$\tfrac{1}{2}\,\mathrm{Tr}(\mathbf{S}) = \mathrm{Re}(S_{11}) = \pm 1. \tag{4.6a}$$

First auxiliary spectrum. The $\{\gamma_i(x_0)\}$, $1 \leqslant i \leqslant N$, are the solutions of

$$\mathrm{Im}(S_{11}) + \mathrm{Im}(S_{21}) = 0. \tag{4.6b}$$

Second auxiliary spectrum. The $\{\eta_i(x_0)\}$, $1 \leqslant i \leqslant N$, are the solutions of

$$\mathrm{Im}(S_{11}) + \mathrm{Re}(S_{21}) = 0. \tag{4.6c}$$

The γ_i and the η_i lie between two discrete eigenvalues ζ_{2j}, ζ_{2j+1}: $\zeta_{2j} \leqslant \gamma_i \leqslant \zeta_{2j+1}$, $\zeta_{2j} \leqslant \eta_i \leqslant \zeta_{2j+1}$. The ζ_{2j}, ζ_{2j+1} are called "band edges." These constraints on the bounds of the auxiliary spectra are exploited below in the numerical simulations.

The *numerical scattering transform spectrum* is computed by the following steps. Given a discrete, complex envelope function $q_n = q(x_n)$ $(0 \leqslant n \leqslant M-1)$, compute the matrix $\mathbf{U}(q_n)$ (4.2) for every n, forming the monodromy matrix $\mathbf{S}(x_0)$ as the product of these matrices by (4.4). Then the spectrum as defined in (4.6) is found by a standard Newtonian root-finding algorithm [50]; the program uses analytic expressions for the derivatives of the matrix (4.2) and of the scattering coefficients with respect to ζ; this allows rapid convergence of the Newton algorithm in (4.6).

The reconstruction of the complex envelope q_n by (3.16) is carried out numerically by computing the auxiliary spectra for the M different base points $x_0 \to x_0, x_1, x_2, \ldots, x_{M-1}$. This is done by computing M different monodromy matrices (4.4) which differ from each other by a shift $n\,\Delta x$ in the potential, q_n (with a corresponding shift in the periodic boundary conditions $q_{M+n} = q_n$). This procedure arises from the following similarity transformation which is easily derived from (4.4):

$$\mathbf{S}(x_{n+1}, \zeta_i) = \mathbf{U}(q_n, \zeta_i)\,\mathbf{S}(x_n, \zeta_i)\,\mathbf{U}(q_n, \zeta_i)^{-1}. \tag{4.7}$$

This expression relates the monodromy matrix $\mathbf{S}(x_{n+1}, \zeta_i)$ at a point x_{n+1} to the previously computed matrix $\mathbf{S}(x_n, \zeta_i)$ at x_n for a particular value of wave number ζ_i. Values of the auxiliary spectra $\{\gamma_i(x_n, \zeta_i),\ \eta_i(x_n, \zeta_i)\}$ for each x_n are computed from the monodromy matrices $\mathbf{S}(x_n)$ by (4.6). Knowledge of the auxiliary spectra at every point x_n allows reconstruction of the complex amplitude function $q(x_n)$ via a discrete version of (3.16):

$$\begin{aligned} q_R(x_n) &= -\tfrac{1}{2}\sum_{j=1}^{2N}\zeta_j + \sum_{i=1}^{N}\eta_i(x_n, \zeta_i) \\ q_I(x_n) &= \tfrac{1}{2}\sum_{j=1}^{2N}\zeta_j - \sum_{i=1}^{N}\gamma_i(x_n, \zeta_i) \end{aligned} \tag{4.8}$$

for $n = 0, 1, 2, \ldots, M-1$, $N = M$. These are finite-term nonlinear generalizations of Fourier series for the discrete envelope function $q(x_n) = q_R(x_n) + iq_I(x_n)$. As indicated by the notation each nonlinear oscillation mode $\{\eta_i, \gamma_i\}$ depends upon the spatial variable x_n and upon the associated wave number ζ_i.

Physical Interpretation and Analysis of Data

The above scenario provides numerical tools for the determination of the IST spectrum and for the reconstruction of the nonlinear wave train from the spectrum. Physically the general solutions to NLS are determined by nonlinear Fourier series of the form (3.16); the discrete representation is given by (4.8). These relations constitute a linear superposition of the nonlinear hyperelliptic oscillation modes of the theory. The hyperelliptic modes reduce to trigonometric functions in the small amplitude, linear limit; therefore periodic IST for NLS may be viewed as a generalization of ordinary Fourier series. The methods as presented here also serve as tools for the nonlinear Fourier analysis of data. In this latter application one determines the nonlinear Fourier spectrum from a measured wave train in order to enhance understanding of its physical behavior [27].

The construction of nonlinear Fourier series also leads naturally to the concept of *nonlinear filtering*. Formally speaking, given a discrete wave train $q(x_n)$, one might wish to remove certain wave number components in order to more closely observe the behavior of others in the space or time domain. The perspective is similar to that for linear filtering, a technique commonly employed using the linear Fourier transform [51]. One removes certain components in the frequency domain and then inverts the transform to obtain the signal without the unwanted components. For example, one might want to filter out high frequency noise or to observe only frequencies in a certain spectral band. Filtering is analogously carried out in the nonlinear case by means of (4.8); one selects the components he wants to remove from the signal and simply deletes them from the sum. The resultant reconstructed wave train no longer contains the unwanted components. This idea was successfully employed in the analysis of ocean surface wave trains to discover the presence of KdV solitons in measured wave data in the Adriatic Sea [29].

The filtering technique just discussed is referred to as a "perfect filter" in analogy with its linear counterpart [51]. The construction of more complex filters, for which special weighting of the nonlinear Fourier amplitudes and phases might be necessary, is not a simple task. Furthermore, different shape filters may be appropriate for different applications. Future work focuses on the development of other kinds of nonlinear filters, methods for their computation, and their respective efficiencies [52].

V. CONSTRUCTION AND ANALYSIS OF NONLINEAR WAVE TRAINS

I now consider a number of exact wave train solutions of the NLS equation, their associated spectral decompositions, and physical interpretations. In each of the examples to be considered I graph (a) the wave train under consideration, (b) the linear Fourier amplitudes of the wave train, (c) the Floquet discriminant of the wave train, $\Delta(\zeta) = \frac{1}{2}\mathrm{Tr}(\mathbf{S})$ as a function of ζ, (d) the nonlinear oscillation modes, $\{\eta_i, \gamma_i\}$, $1 \leqslant i \leqslant N$, and (e) the reconstructed wave train using the linear superposition law (4.8). The following examples serve to illustrate the method, provide for checkout of the program, and enhance the physical understanding of the defocusing NLS equation.

Plane Wave Solutions and Numerical Convergence

The first numerical example consists of the computation of the spectrum associated with a simple plane wave $q(x) = q_0 e^{ikx}$, for which the scattering transform spectrum is analytically known [11]. The main spectrum has one open band ($N = 1$) and is given by

$$\zeta_1 = -\frac{k}{2} + q_0, \qquad \zeta_2 = -\frac{k}{2} - q_0. \tag{5.1}$$

Note that the amplitude of the open band ($\zeta_2 - \zeta_1 = 2q_0$) is twice the amplitude of the envelope function q_0. The algorithm assumes a piecewise constant envelope function $q(x_n)$, which is, after all, an imperfect representation of the continuous function $q(x, 0)$ as a solution to NLS. I have compared the numerically computed amplitudes ($2q_{0,\mathrm{com}}$) with the exact analytical results (5.1) to assess the behavior of the algorithm. Numerical tests on the convergence of the algorithm with respect to the discrete inverse scattering transform of Ablowitz and Ladik [53] (as here adapted to the periodic problem, see (5.2) below) (Fig. 2) have also been conducted. Graphed is the numerically computed relative error ($\varepsilon = 2\,|q_0 - q_{0,\mathrm{com}}|/q_0$) as a function of the number of discretization points M. Both algorithms are seen to give dramatic improvement in accuracy with increasing M. However, the algorithm given herein improves at a faster

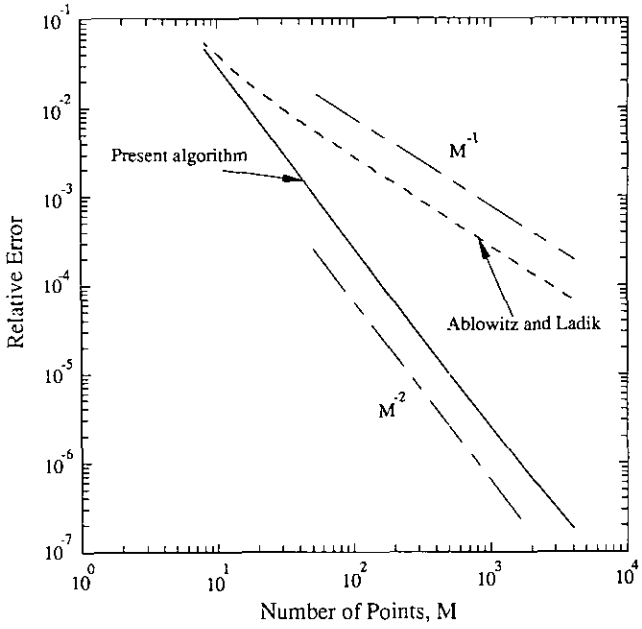

FIG. 2. Comparison of the rates of convergence of the periodic direct scattering transform given herein with the discrete algorithm of Ablowitz and Ladik [53] wich has been adapted from the infinite-line problem to the periodic problem as discussed in Section 5. The logarithm of the relative error in the open band width of a plane wave (Eq. (5.1)) is graphed as a funcion of the logarithm of the number of discretization intervals M; Ablowitz and Ladik (---) and presents results (———). Lines with slopes M^{-1} (resembling Ablowitz and Ladik) and M^{-2} (resembling the present approach) are also shown.

rate. The error for the Ablowitz and Ladik algorithm decreases as a power law M^{-1} while the present algorithm decreases as M^{-2} for increasing M. This occurs in part because the scattering matrix of Ablowitz and Ladik may be obtained from the scattering matrix (4.2) by a leading order Taylor expansion in $k\,\Delta x$:

$$\mathbf{U}(q) \cong \begin{pmatrix} 1 - i\zeta\,\Delta x & q\,\Delta x \\ q^*\,\Delta x & 1 + i\zeta\,\Delta x \end{pmatrix}. \tag{5.2}$$

This latter matrix, which arose originally from discrete, infinite-line scattering theory [53], has been employed in the above simulations for comparison to Ablowitz and Ladik; i.e., the matrix (4.2) has been replaced by (5.2) in the periodic formulation. The present work evidently sets the stage for the future development of algorithms with a wide range of forms for the matrix $\mathbf{U}(q)$ which will probably depend upon the simultaneous requirements of speed and precision. For example, one might extend the Taylor series approximation of (4.2) to higher order than given by (5.2) or one might consider a piecewise linear approximation of the potential, for which (4.2) contains Airy functions.

It should be remembered that the new algorithm given herein provides a numerical approach for computing an *estimate* of the scattering spectrum of the *continuous*,

periodic NLS equation as described by Ma and Ablowitz [11]. Alternatively the approach of Ablowitz and Ladik [53] provides an *exact* theory of inverse scattering for discrete envelope functions of the associated *discrete NLS equation* with infinite-line boundary conditions.

The method given here may be viewed as associated with a discrete, periodic NLS-type equation of higher order than that given in [53]. The new approach is *not* integrable by IST because of the specific form (4.2) of **U**, but the numerical characteristics of the algorithm are quite good; replacement of the matrix **U** in the present algorithm by the matrix of (5.2) makes the method consistent with Ref. [53] but this reduces the numerical accuracy as the results of Fig. 2 show.

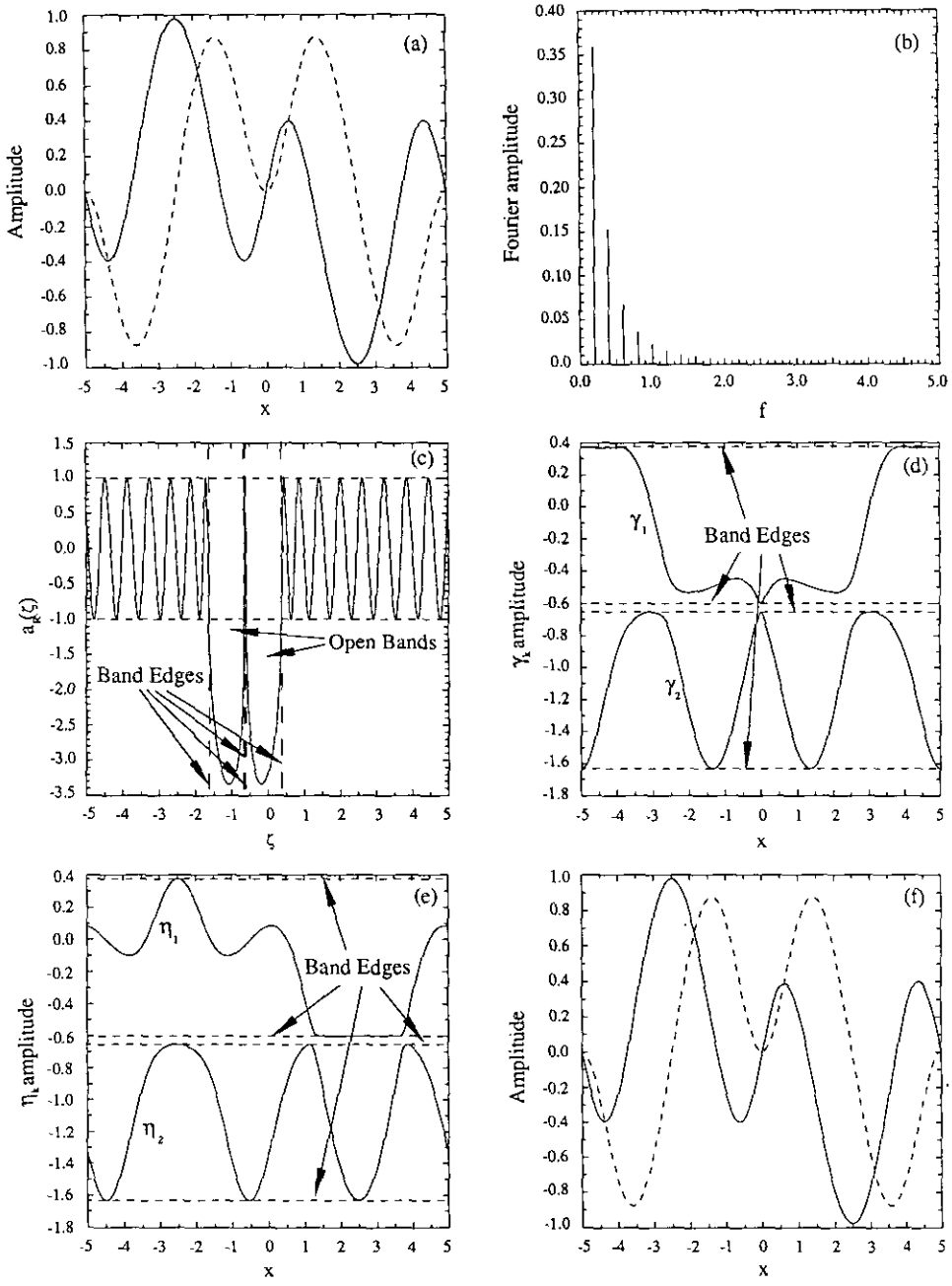

FIG. 3. Snoidal wave simulation, $m = 0.900$, $k = 4\pi/L$, $L = 10$, and $M = 512$. In panel (a) are the real (———) and imaginary (– – –) parts of the envelope function. The linear Fourier amplitudes are shown in panel (b). The Floquet diagram shows two open bands ($N = 2$) in the spectrum (c). The spatial evolution of the two hyperelliptic functions γ_1, γ_2 is shown in (d). The spatial evolution of the hyperelliptic functions η_1, η_2 is given in (e). The horizontal dotted lines denote the band edges in (d) and (e). Finally in (f) the wave envelope is reconstructed (by Eq. (4.8)) using the two hyperelliptic function solutions in (d), (e).

Snoidal Wave Simulations

The NLS equation has the *snoidal wave envelope solution* [27],

$$q(x) = q_0 e^{ikx} \operatorname{sn}(px|m) \tag{5.3}$$

where $p = 4K(m)/L$. $K(m)$ is the elliptic integral, L is the period, $q_0 = \sqrt{m}\, p$, and m is the modulus. The solution (5.3) has two "open bands" in the Floquet spectrum. The first case considered has $m = 0.900$ (Fig. 3), where panel (a) shows the real (q_R, ———) and imaginary (q_I, – – –) parts of the complex envelope function. The Fourier transform of the envelope function given in Fig. 3a is shown in Fig. 3b. The Floquet discriminant is graphed in Fig. 3c as a function

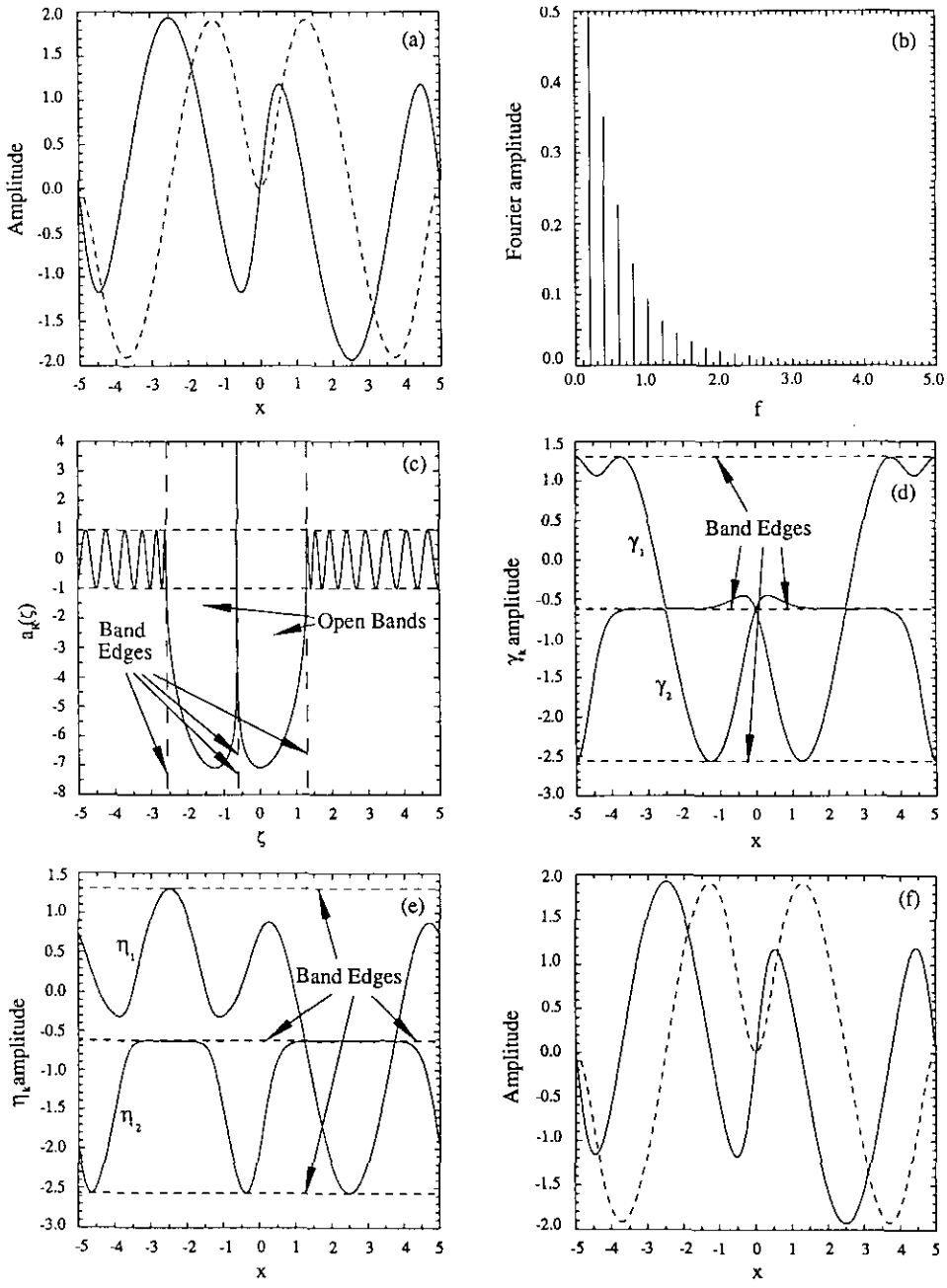

FIG. 4. Snoidal wave simulation, $m = 0.999$, $k = 4\pi/L$, $L = 10$, and $M = 512$. In panel (a) are the real (———) and imaginary (– – –) parts of the envelope function. The linear Fourier amplitudes are shown in panel (b). The Floquet diagram shows two open bands ($N = 2$) in the spectrum (c). The spatial evolution of the two hyperelliptic functions γ_1, γ_2 is shown in (d). The spatial evolution of the hyperelliptic functions η_1, η_2 is given in (e). The horizontal dotted lines denote the band edges in (d) and (e). Finally in (f) the wave envelope is reconstructed (by Eq. (4.8)) using the two hyperelliptic function solutions in (d), (e).

of ζ, where two open bands are clearly evident. The hyperelliptic functions γ_1, γ_2 are given in Fig. 3d while η_1, η_2 are shown in Fig. 3e. Finally the superposition formulas (4.8) are used to reconstruct the complex envelope q (Fig. 3f), which accurately agrees with the input wave form given in Fig. 3a. For the present example the input wave form is reproduced to eight significant figures. Double precision arithmetic was used in the program; the Newtonian search for the zeros in Eqs. (4.6) was terminated when the difference between successive zeros dropped below 10^{-10}; improved precision occurs upon reducing this value.

A more nonlinear snoidal wave case is considered in Fig. 4 for which $m = 0.999$. In panel (a) the real and imaginary parts of the envelope q_R (———), q_I (– – –) are

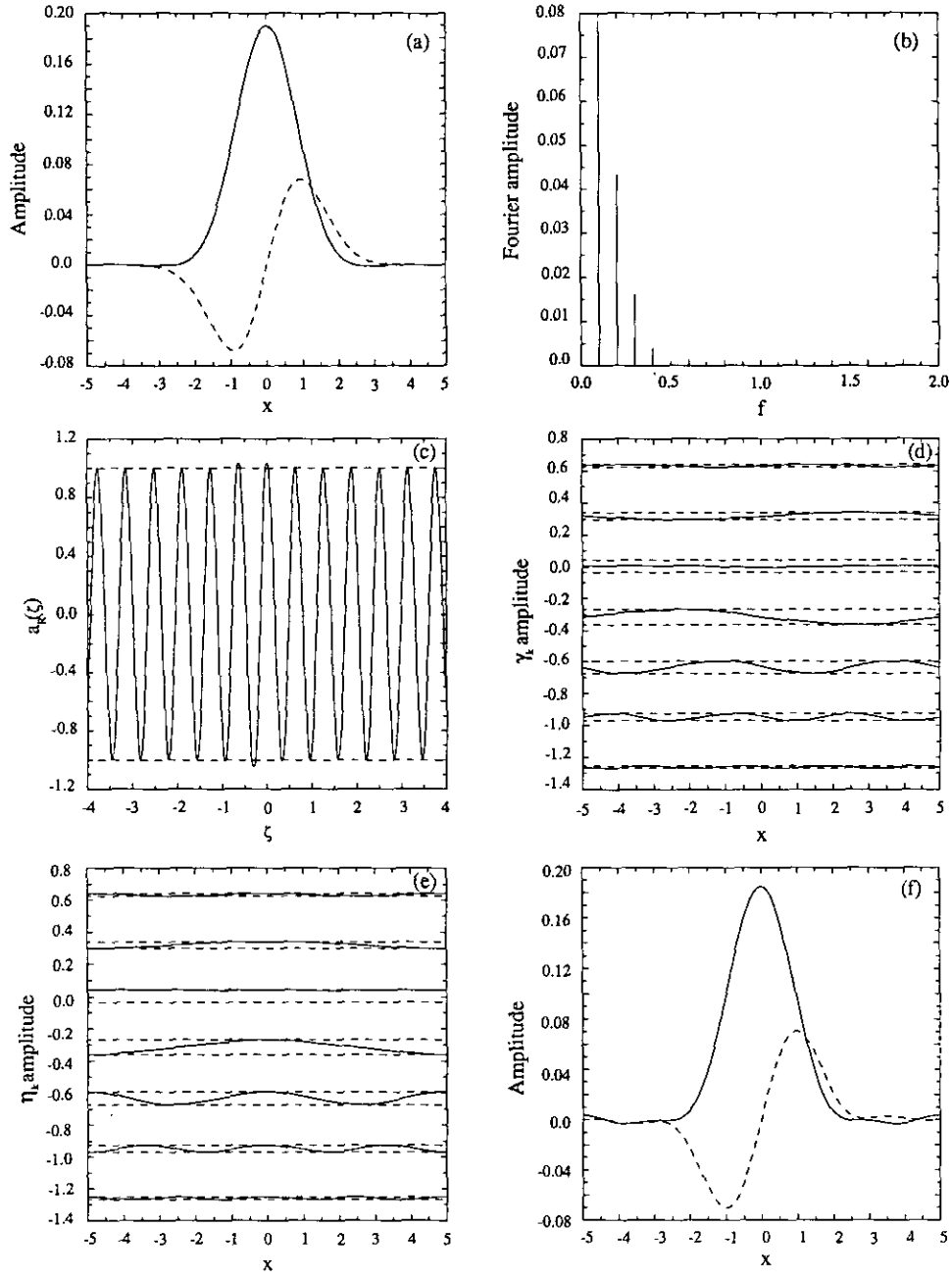

FIG. 5. Gaussian wave packet simulation, $q_0 = 0.19$, $\sigma_0 = 2$, $k = 2\pi/L$, $L = 10$, and $M = 512$. In panel (a) are shown the real (———) and imaginary (– – –) parts of the envelope function. The linear Fourier components are given in panel (b). The Floquet diagram shows several small open bands in the spectrum (c). The spatial evolution of the hyperelliptic functions γ_i is shown in (d). The spatial evolution of the hyperelliptic functions η_i is given in (e). The horizontal dotted lines denote the band edges in (d) and (e). Finally, in (f) the wave envelope is reconstructed (by Eq. (4.8)) using the two hyperelliptic function solutions in (d), (e).

given. The Fourier transform of the envelope function is shown in Fig. 4b. From Fig. 4c one sees that two large bands are open in the spectrum. The spatial evolutions of γ_1, γ_2 (Fig. 4d) and η_1, η_2 (Fig. 4e) are seen to be more complex than in Fig. 3. In fact these functions occasionally "stick" to and remain constant on a band edge (horizontal dotted lines in Figs. 4d, e), a phenomena also seen in the nonlinear dynamics of the KdV equation [23]. Using Eq. (4.8), the inverse scattering transform gives the reconstructed wave train in panels (f) (real part q_R,

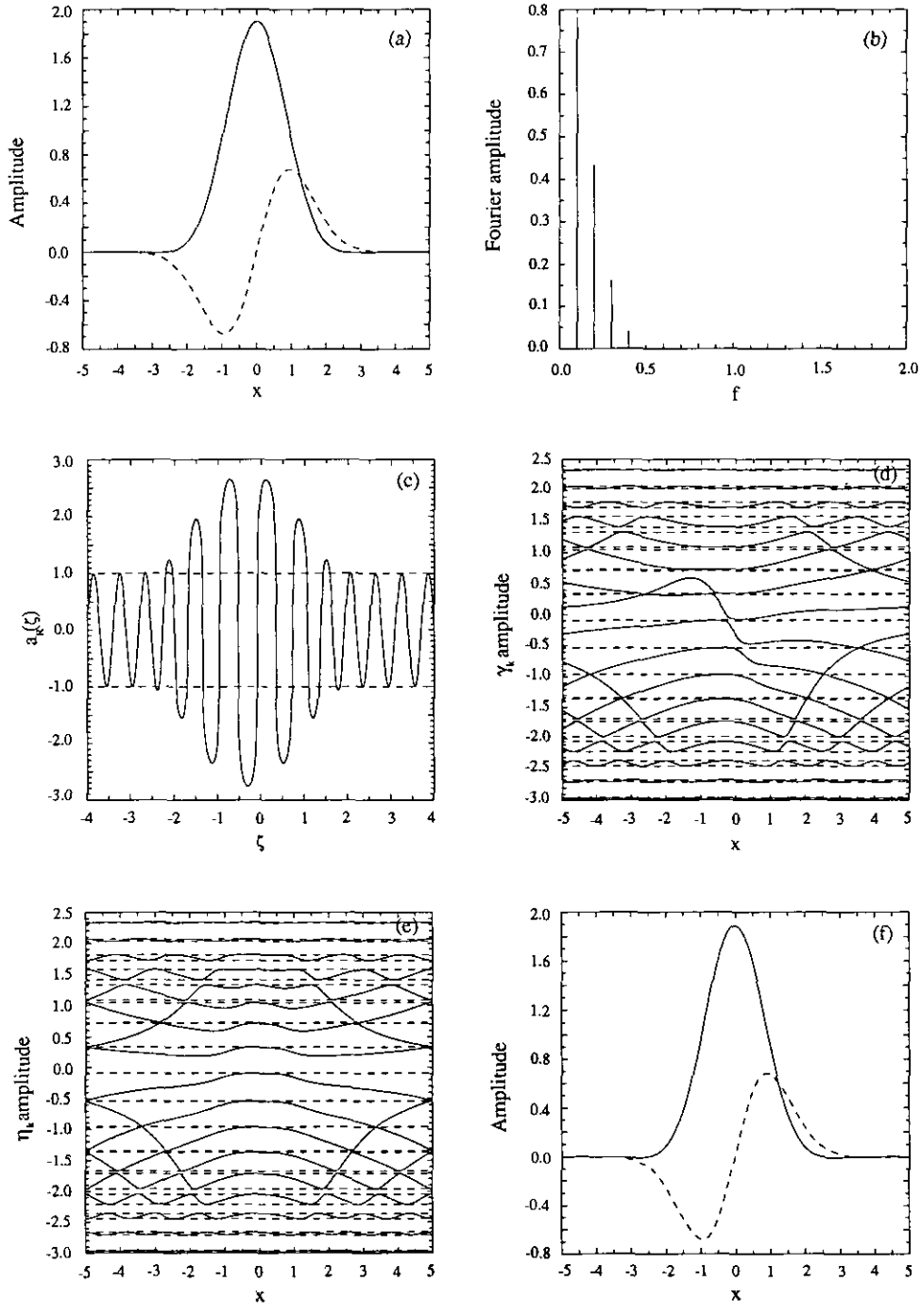

FIG. 6. Gaussian wave packet simulation, $q_0 = 1.9$, $\sigma_0 = 2$, $k = 2\pi/L$, $L = 10$, and $M = 512$. In panel (a) are the real (———) and imaginary (– – –) parts of the envelope function. The linear Fourier amplitudes are given in panel (b). The Floquet diagram shows several large open bands in the spectrum (c). The spatial evolution of the 17 hyperelliptic functions γ_i is shown in (d). The spatial evolution of the hyperelliptic functions η_i is given in (e). The horizontal dotted lines denote the band edges in (d) and (e). Finally, in (f) the wave envelope is reconstructed (by Eq. (4.8)) using the hyperelliptic function solutions in (d), (e).

———), (g) (imaginary part q_I, – – –) of Fig. 4. The reconstruction process is found to reproduce the input wave train in Fig. 4a to good precision, approximately eight significant figures.

The above two examples suggest that nonlinear Fourier theory is substantially more complex than linear Fourier theory. Nevertheless, using the numerical methods given herein, it is quite straightforward to obtain the IST spectrum and to reconstruct the nonlinear wave train.

Gaussian Wave Packet Simulations

I now study a more complex situation in which propagating *nonlinear Gaussian wave packets* are considered. The form of a wave packet is taken to be

$$q(x) = q_0 e^{ikx} e^{-x^2/\sigma_0}, \tag{5.4}$$

where q_0 is the amplitude and σ_0 is the half-width of the pulse. The first case has a relatively small amplitude, $q_0 = 0.19$. The real and imaginary parts of the Gaussian packet are shown in Fig. 5a. The linear Fourier transform of the packet is given in Fig. 5b. The Floquet diagram, Fig. 5c, shows that the wave train is essentially linear; i.e., the open bands are small in width and few in number. The representations for the hyperelliptic functions γ_i are presented in panel (d); one can see that each of the degrees of freedom is fairly sinusoidal, a further indication of the small-amplitude, linear character of this example. The hyperelliptic functions η_i are shown in panel (e); these too are nearly sinusoidal in appearance. I have used the largest seven hyperelliptic oscillation modes to reconstruct the original wave train and the results are shown in panel (f). Note that by including only the first seven modes the reconstruction is not quite perfect, as can be seen in the tails of the Gaussian function. Improved agreement is obtained by including higher order modes in the reconstruction process. These results parallel linear Fourier analysis.

In order to better understand the influence of enhanced nonlinear effects I have considered another Gaussian packet for which the amplitude is ten times larger than in Fig. 5, $q_0 = 1.9$. The real and imaginary parts of the Gaussian are shown in Fig. 6a. The Fourier transform of this complex envelope function is given in Fig. 6b. The Floquet spectrum (Fig. 6c) is now quite different than the preceding case; i.e., the number and size of the open bands has grown considerably. Also shown are the largest seventeen oscillation modes: the γ_i are given in Fig. 6d while the η_i are shown in Fig. 6e. Note in particular that adjacent hyperelliptic functions actually meet at the band edges for the largest (most energetic) of the modes, an effect seen previously in the example of Fig. 4. The largest nonlinear mode lies near the values γ, $n \sim 0$ and the other modes lie further away (above and below zero in Figs. 6d, e) and are smaller in amplitude and higher in frequency (i.e., the open band widths in Fig. 6c decrease as one moves away from the values γ, $\eta \sim 0$). The observation that the number of oscillations of the hyperelliptic functions increases as the amplitude decreases also holds true for the linear Fourier transform representation of the Gaussian packet. The first 17 nonlinear modes are used to reconstruct the original wave in Fig. 6f. Some faint oscillations occur in the tail of the Gaussian primarily because I have taken only a small number of nonlinear Fourier modes in the reconstruction process; increasing the number of modes increases the precision.

VI. CONCLUSIONS

I have developed numerical methods for computing both the *direct* and *inverse scattering transforms* for the defocusing nonlinear Schroedinger equation. The approach is based upon a piecewise constant representation for the complex envelope function of NLS, for which one computes the Floquet spectrum (Eq. (4.6a)) and the hyperelliptic function oscillation modes (Eqs. (4.6b), (4.6c)). A linear superposition of the oscillation modes using (4.8) allows one to reconstruct the wave train or to nonlinearly filter noise or other undesirable components. It is expected that one of the most important applications of the algorithm will be the analysis of nonlinear wave data in both laboratory and field conditions.

It is worthwhile discussing certain results relating to nonlinear filtering applications of the algorithms given herein (see analogous considerations for the KdV equation in Refs. [25–27, 29–31]). One can ask: What influence do nonlinear interactions have on a filtering procedure which is based upon the linear superposition law (4.8)? Due to nonlinear interactions each hyperelliptic function influences the behavior of all the others and one would further expect the nearest-neighbor interactions to be of prime importance. It should therefore not be surprising that the arbitrary removal of certain strongly interacting spectral components may influence the outcome of the filtering process. This is, in fact, what one finds numerically. Generally speaking an *iterative filtering process must be carried out to reduce the* effect of nonlinear interactions, particularly *outside* the frequency range of interest; i.e., deleting certain hyperelliptic functions in (4.8) (outside a particular frequency range, a *band pass filter*) does not generally remove all of the influence of the nonlinear interactions and a second or third filtering operation must be carried out in order to remove additional high frequency energy. This effect was noted by Osborne *et al.* [29] in the analysis of oceanic wave data using the scattering transform for the periodic KdV equa-

tion; two filtering iterations enabled the removal of the radiation spectrum to allow observation of the soliton component in a measured oceanic wave train.

The reader may further ask why the *focusing* case has not been addressed in the present paper. This topic deserves a separate paper in its own right, dedicated to the details of the behavior of the *non-self-adjoint* spectral problem and to the hyperelliptic inverse problem for the focusing NLS equation. There are several technical issues which require lengthy discussion. The hyperelliptic functions generally do not lie inside the open bands in the spectrum but are free to wander anywhere in the complex plane. Numerically this requires additional nontrivial code to find zeros in the complex plane and to follow the spatial dynamics of the hyperelliptic functions without having the convenient constraint that they be confined within the open bands, as for the defocusing case. This behavior is deeply linked to the problem of instabilities in focusing NLS. Additionally, the problem of high order poles in the focusing problem is crucial, since second (or higher) order poles may contribute to the spectrum and consequently need to be included in the inverse problem. The analysis considered herein covers C^∞ initial values of the Cauchy problem for defocusing NLS; however, for the focusing case this issue is far from being completely resolved, suggesting that the inverse problem may not be able to construct *all* potentials of the *focusing* NLS equation. These issues require considerable care and it seems appropriate to put the results in a separate paper where they can be given adequate attention.

ACKNOWLEDGMENTS

I acknowledge the continuing invaluable support of Professor L. Bergamasco. This work is supported in part by Office of Naval Research Grant N00014-92-J-1330.

REFERENCES

1. M. J. Ablowitz, D. J. Kaup, A. C. Newell, and H. Segur, *Stud. Appl. Math.* **53**, 249 (1974).
2. C. S. Gardner, J. M. Greene, M. D. Kruskal, and R. M. Miura, *Phys. Rev. Lett.* **19**, 1095 (1967).
3. V. E. Zakharov and A. B. Shabat, *Sov. Phys. JETP* **34**, 62 (1972).
4. M. J. Ablowitz and H. Segur, *Solitons and the Inverse Scattering Transform* (SIAM, Philadelphia, 1981).
5. S. P. Novikov, *Funct. Anal. Appl.* **8**, 236 (1974).
6. B. A. Dubrovin and S. P. Novikov, *Sov. Phys. JETP* **40**, 1058 (1974).
7. H. P. McKean and P. VanMoerbeke, *Invent. Math.* **30**, 217 (1976).
8. H. P. McKean and E. Trubowitz, *Commun. Pure Appl. Math.* **29**, 143 (1976).
9. A. R. Its and V. B. Matveev, *Funct. Anal. Appl.* **9**, 65 (1976).
10. B. A. Dubrovin, V. B. Matveev, and S. P. Novikov, *Russian Math. Surv.* **31**, 59 (1976).
11. Y. C. Ma and M. J. Ablowitz, *Stud. Appl. Math.* **65**, 113 (1981).
12. M. G. Forest and D. W. McLaughlin, *J. Math. Phys.* **23**, 1248 (1982).
13. V. E. Zakharov, S. V. Manakov, S. P. Novikov, and M. P. Pitayevsky, *Theory of Solitons. The Method of the Inverse Scattering Problem* (Nauka, Moscow, 1980) [Russian].
14. R. K. Dodd, J. C. Eilbeck, J. D. Gibbon, and H. C. Morris, *Solitons and Nonlinear Wave Equations* (Academic Press, London, 1982).
15. A. C. Newell, *Solitons in Mathematics and Physics* (SIAM, Philadelphia, 1985).
16. A. Degasperis, "Nonlinear Wave Equations Solvable by the Spectral Transform," in *Nonlinear Topics in Ocean Physics*, edited by A. R. Osborne (Elsevier, Amsterdam, 1989).
17. A. R. Osborne, "The Spectral Transform: Methods for the Fourier Analysis of Nonlinear Wave Data," in *Statics and Dynamics of Nonlinear Systems*, edited by G. Benedek, H. Bilz, and R. Zeyher (Springer-Verlag, Berlin, 1983).
18. A. R. Osborne and L. Bergamasco, *Nuovo Cimento B* **85**, 2293 (1985).
19. A. R. Osborne, in preparation, 1993 (unpublished).
20. A. R. Osborne and L. Bergamasco, *Physica D* **18**, 26 (1986).
21. E. R. Tracy, J. W. Larson, A. R. Osborne, and L. Bergamasco, *Physica D* **32**, 83 (1988).
22. A. R. Osborne and G. Boffetta, *Phys. Fluids A* **1**, 1200 (1989).
23. A. R. Osborne and E. Segre, *Physica D* **44**, 575 (1990).
24. E. R. Tracy, J. W. Larson, A. R. Osborne, and L. Bergamasco, in *Nonlinear Topics in Ocean Physics*, edited by A. R. Osborne (North-Holland, Amsterdam, 1991).
25. A. R. Osborne, *J. Comput. Phys.* **94** (2), 284 (1991).
26. A. Provenzale and A. R. Osborne, *J. Comput. Phys.* **94** (2), 314 (1991).
27. A. R. Osborne, in *Nonlinear Topics in Ocean Physics*, edited by A. R. Osborne (North-Holland, Amsterdam, 1991).
28. A. R. Osborne and E. Segre, *Physica D* **44**, 575 (1990).
29. A. R. Osborne, E. Segre, G. Boffetta, and L. Cavaleri, *Phys. Rev. Lett.* **64** (15), 1733 (1991).
30. G. Boffetta, A. R. Osborne, M. Petti, and E. Segre, in *Nonlinear Ocean Waves*, edited by A. Brandt, S. E. Ramberg, and M. F. Shlesinger (World Scientific, Singapore, 1992).
31. A. R. Osborne and M. Petti, *Phys. Rev. E* **47** (2), 1035 (1993).
32. W. E. Ferguson, Jr., H. Flaschka, and D. W. McLaughlin, *J. Comput. Phys.* **45**, 157 (1982).
33. A. R. Bishop, M. G. Forest, D. W. McLaughlin, and E. A. Overman II, *Physica D* **18**, 293 (1986).
34. M. G. Forest and J.-E. Lee, in *Oscillation Theory, Computation and Methods of Compensated Compactness*, IMA in Mathematics and its Applications, Vol. 2 (Springer-Verlag, Berlin, 1986), p. 35.
35. A. R. Bishop and P. S. Lomdahl, *Physica D* **18**, 54 (1986).
36. G. Terrones, D. W. McLaughlin, E. A. Overman II, and A. Pearlstein, *SIAM J. Appl. Math.* **50**, 791 (1990).
37. N. M. Ercolani, M. G. Forest, and D. W. McLaughlin, *Physica D* **43**, 349 (1990).
38. M. J. Ablowitz and B. M. Herbst, in *Hamiltonian Systems, Transformation Groups and Spectral Transform Methods*, edited by J. Harnad and J. E. Marsden (CRM, Montreal, 1990).
39. M. J. Ablowitz, B. M. Herbst, and J. A. C. Weideman, *IMA J. Numer. Anal.* **11**, 539 (1991).
40. R. Flesch, M. G. Forest, and A. Sinha, *Physica D* **48**, 169 (1991).
41. D. W. McLaughlin and C. M. Schober, *Physica D* **57**, 447 (1992).
42. V. E. Zakharov and E. A. Kuznetsov, *Physica D* **18**, 455 (1986).

43. V. E. Zakharov, *J. Appl. Mech. Tech. Phys.* **2**, 190 (168).
44. H. Hasimoto and H. Ono, *J. Phys. Soc. Jpn.* **33**, 805 (1972).
45. H. C. Yuen and B. M. Lake, *Annu. Rev. Fluid Mech.* **12**, 303 (1980).
46. H. C. Yuen and B. M. Lake, *Adv. Appl. Mech.* **22**, 67 (1982).
47. H. C. Yuen, in *Topics in Ocean Physics*, edited by A. R. Osborne and P. Malanotte Rizzoli (North-Holland, Amsterdam, 1982).
48. H. C. Yuen, in *Nonlinear Topics in Ocean Physics*, edited by A. R. Osborne (North-Holland, Amsterdam, 1991).
49. G. B. Whitham, *Linear and Nonlinear Waves* (Interscience, New York, 1974).
50. G. Boffetta and A. R. Osborne, *J. Comput. Phys.* **102**, 252 (1992).
51. J. S. Bendat and A. G. Piersol, *Random Data: Analysis and Measurement Procedures* (Wiley-Interscience, New York, 1971).
52. A. R. Osborne, in preparation, 1993 (unpublished).
53. M. J. Ablowitz and J. Ladik, *J. Math. Phys.* **16**, 598 (1975); **17**, 1011 (1976).